Substituent Effects in Cluster Species. 3. Structural Consequences of Intercage π Interactions in the Dimer and Trimer of 1,5-$C_2B_3H_5$

E. L. Andersen, R. L. DeKock,[1] and T. P. Fehlner*

Contribution from the Department of Chemistry, University of Notre Dame, Notre Dame, Indiana 46556. *Received October 4, 1979*

Abstract: The dimer, 2,2′-[1,5-$C_2B_3H_4]_2$, and trimer, 2,2′-3,2′-[1,5-$C_2B_3H_4]_2$-1,5-$C_2B_3H_3$, of 1,5-$C_2B_3H_5$ have been prepared by the pyrolysis of the monomer. Both compounds have been characterized experimentally by NMR, IR, and UV photoelectron spectroscopy and the dimer by Raman spectroscopy as well. The structure of the dimer and the structure of the trimer have been explored using the MNDO quantum chemical approach. The experimental and calculational results clearly show that the dimer and trimer consist of 1,5-$C_2B_3H_x$ units coupled by one and two exopolyhedral B–B bonds and demonstrate that, with respect to rotation around the B–B bond, the dimer possesses a single stable conformation that has D_{2d} symmetry. The MNDO calculations show that the observed geometry results from a π-type interaction across the exopolyhedral B–B bond. This intercage interaction is similar to that observed previously between cage surface orbitals and π substituents.

Both boron and carbon exhibit a characteristic facility toward catenation; however, the boranes usually feature three-dimensional polyhedra rather than the chains and rings of carbon chemistry. The possibility of making chains of cages results from the discovery in 1961 by Grimes et al.[2] of two cages joined by an exopolyhedral boron–boron bond. Since that time further examples of coupled boranes[3-10] and heteroboranes[11-16] have been reported and recent work from several laboratories has demonstrated that selective coupling of borane and carborane cages in good yield is possible.[17,18]

We have previously studied the nature of the interaction of exopolyhedral substituents with π-type[19,20] filled orbitals and have demonstrated that the major interaction observed by photoelectron spectroscopy is with the surface (π) orbitals of the cage. We have now studied the spectroscopic and calculated properties of 2,2′-[1,5-$C_2B_3H_4]_2$ and 2,2′-3,2′-[1,5-$C_2B_3H_4]_2$-1,5-$C_2B_3H_3$, the dimer and trimer of 1,5-$C_2B_3H_5$. The information obtained demonstrates that a similar π interaction of orbitals across the B–B bond is revealed by and reflected in the relative orientation of the cages.

Experimental Section

Materials and Equipment. NMR spectra were recorded on a Varian XL-100 spectrometer under the following conditions: ^{11}B, FT at 32.1 (field locked) or 25.2 (field unlocked) MHz; ^{1}H, FT at 100 MHz; in CD_2Cl_2. Mass spectra were obtained using an AEI MS-902 mass spectrometer. The infrared spectra were recorded in the gas phase on a Perkin-Elmer 457 spectrometer and the Raman spectra were obtained in the liquid state on a Spex laser Raman spectrometer at 514.5 nm. Photoelectron spectra were recorded in the gaseous state using He(I) (21.2 eV) and, in some cases, Ne(I) (16.8 eV) radiation. The spectrometer[21] was operated at a resolution of 20 meV (fwhm) at 5 eV electron energy and the spectra were calibrated using an internal standard of argon and xenon.

The starting material, 1,5-$C_2B_3H_5$, was purchased from Chemical Systems, Inc., Irvine, Calif. All other reagents were reagent grade. Purifications, reactions, and product separations were carried out using standard high-vacuum procedures.[22] Pyrolyses were performed in a standard, Pyrex "hot-cold" reactor equipped with a Teflon stopcock.[23] The center tube was heated with a sand bath and the outside tube was cooled in a water bath.

Polymerization of 1,5-$C_2B_3H_5$. In a typical reaction, the reactor was charged with 5.7 mmol of 1,5-$C_2B_3H_5$ and placed in an ice bath and the center heated to 400 °C for 4 h. The reactor was cooled with liquid nitrogen and the hydrogen (0.8 mmol) was removed. Fractionation of the volatiles yielded 4.3 mmol of 1,5-$C_2B_3H_5$ at −196 °C, 0.3 mmol of I at −95 °C,[24] and a trace of II at −30 °C.[25] The mass spectrum of I yielded the molecular formula $C_4B_6H_8$ ($^{12}C_4{}^{11}B_6{}^1H_8{}^+$; calcd 122.118, obsd 122.118 amu). The distribution of ion intensities in the parent envelope was consistent with six borons and little fragmentation was observed. The mass spectrum of II yielded the molecular formula $C_6B_9H_{11}$ ($^{12}C_6{}^{11}B_9{}^1H_{11}{}^+$; calcd 182.170, obsd 182.170 amu). The distribution of ion intensities in the parent envelope was consistent with nine borons and little fragmentation was observed. The gas-phase infrared spectrum of II (at its vapor pressure at 25 °C, which is about 1 Torr) exhibited bands at 2525 sh, 2515 m (both BH), and 1112 sh and 1106 m (both framework) cm^{-1}. The yield of I based on consumed 1,5-$C_2B_3H_5$ was 41%.

Reaction of $C_4B_6H_8$ with $Fe(CO)_5$. The reaction of I with $Fe(CO)_5$ in the "hot-cold" reactor (200 and 40 °C) followed by fractionation produced small amounts of $C_4B_6H_8Fe(CO)_3$. The mass spectrum of a pure sample exhibits a parent envelope consistent with six borons and fragmentation consistent with the loss of three CO molecules. The molecular formula was defined by precise mass measurement ($^{56}Fe^{12}C_7{}^{11}B_6{}^{16}O_3{}^1H_8{}^+$; calcd 262.038, obsd 262.040 amu) but lack of material precluded further characterization. This experiment demonstrates that the individual dimer cages behave chemically as the monomer.[26]

Calculations. Calculations on the neutral carboranes of interest were carried out on an IBM 370/168 computer using the MNDO method.[27] Calculations on selected ions were carried out on the Calvin College Prime 400 computer. As a control, two calculations were completed for 1,5-$C_2B_3H_5$: one on the experimental geometry and one on the MNDO optimized geometry. The results obtained at Notre Dame optimized to a slightly lower energy than those of Dewar and McKee[28] (26.8 vs. 27.5 kcal mol^{-1} for $\Delta H_f°$) and the MNDO geometry agrees well with the experimental except that the B–B distance is overestimated by 0.1 Å. The two sets of calculated eigenvalues agree closely except for the a_2'' (CH) orbital (Δ = 0.6 eV), which appears sensitive to geometry. The agreement of these results with a set of ab initio[29] and PRDDO[30] calculations is reasonable. The correspondence between the calculated eigenvalues and the assigned PES results[31] is typical assuming Koopmans' theorem.[32] The MNDO calculations predict the IPs at too high energy, roughly 1–3 eV in the range 10–20 eV. The most noticeable disagreement between theory and experiment is in the assignment of the a_2'' (CH) in that the MNDO calculated IP is 1–2 eV low compared to the other levels. This discrepancy carries through to the dimer and trimer and, as it is known that the a_2'' eigenvalue is sensitive to geometry (see above), the experimental assignments are retained in cases of calculated orbital inversions. With this exception, Koopmans' theorem is used to discuss the results.

Numerous MNDO calculations were done on 2,2′-[1,5-$C_2B_3H_4]_2$ in D_{2h}, D_{2d}, and intermediate D_2 symmetries using the coordinate system shown at the bottom of Figure 6. Within the confines of the specified symmetries, all bond lengths and bond angles were optimized. Searches were made for stable lower symmetry structures of C_{2h} symmetry but none were found. Nevertheless, one can never be completely sure that the most stable geometry has been found. This problem has been discussed by Dewar and McKee.[33] Similar, but not as many, calculations were carried out on 2,2′-3,2′-[1,5-$C_2B_3H_4]_2$-1,5-$C_2B_3H_3$.

0002-7863/80/1502-2644$01.00/0

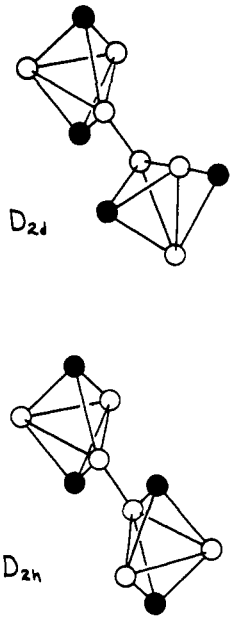

Figure 1. The D_{2d} and D_{2h} conformations of 2,2′-[1,5-$C_2B_3H_4$]$_2$. Each closed circle represents CH and each open circle BH or B.

Table I. 32.1-MHz ^{11}B FT NMR Spectra[a]

compd	δ,[b] ppm		assignment[e]
2,2′-[1,5-$C_2B_3H_4$]$_2$	8.7 (s)[c]	area 2	B 2,2′
	1.8 (d) [J = 190][d]	area 4	B 3,3′,4,4′
2,2′-3,2′-[1,5-$C_2B_3H_4$]$_2$-1,5-$C_2B_3H_3$	7.7 (s)	area 4	B 2,3,2′,2″
	1.5 (d) [J = 170]	area 5	B 4,3′,3″,4′,4″

[a] In CD_2Cl_2 solution. [b] Relative to $BF_3{\cdot}O(C_2H_5)_2$ = 0.0. [c] d = doublet, s = singlet. [d] Coupling constant in hertz. [e] Verified by ^{1}H decoupling.

Table II. 100-MHz ^{1}H FT NMR Spectra[a]

compd	δ,[b] ppm		assignment
2,2′-[1,5-$C_2B_3H_4$]$_2$	4.0 (q)[c] [J = 188][d]		BH
	5.9 (s)		CH
2,2′-3,2′-[1,5-$C_2B_3H_4$]$_2$-1,5-$C_2B_3H_3$	3.5 (s)[e] } 3.7 (s)[e] }	area 5	BH
	5.7 (t)[e] [J = 2.0]	area 4	
	5.8 (d)[e] [J = 1.9]	area 2	CH

[a] In CD_2Cl_2 solution. [b] Relative to Me_4Si = 0.0. [c] q = quartet, t = triplet, d = doublet, s = singlet. [d] Coupling constant in hertz. [e] ^{11}B decoupled.

Results and Discussion

Structural Characterization. The ^{11}B and ^{1}H NMR data for the dimer and trimer of 1,5-$C_2B_3H_5$ are given in Tables I and II, respectively. The data on $C_4B_6H_8$ are consistent with those reported previously[13,14] and support a structure consisting of two $C_2B_3H_4$ cages coupled via an exopolyhedral boron–boron bond. The ^{11}B spectrum of $C_6B_9H_{11}$ indicates that four of the boron atoms do not have hydrogen atoms directly bonded to them while the other five borons have a single terminal hydrogen. The ^{1}H spectrum indicates two types of CH hydrogens in the ratio of 2:4, the peak of area 2 being a doublet with coupling constant 1.9 Hz and the peak of area 4 being a triplet with coupling constant 2.0 Hz. On boron decoupling, two overlapping singlets of total area 5 are observed as well. As the ^{1}H spectrum of 1,5-$C_2B_3H_5$[34] exhibits a CH resonance at δ 5.50, J(HCBH) = 2.1 Hz, and a BH resonance at δ 3.83, it seems clear that $C_6B_9H_{11}$ consists of three C_2B_3 cages linked by exopolyhedral boron–boron bonds. The CH resonance at δ 5.8, which is split by one BH proton, is assigned to the center cage while the CH resonance at δ 5.7, which is split by two BH protons, is assigned to the two equivalent end cages. The relative peak areas are in agreement with this assignment.

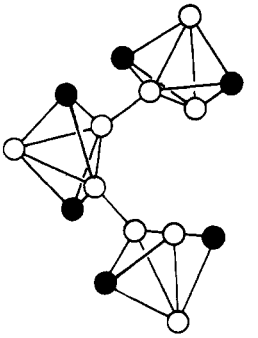

Figure 2. The C_{2v} staggered–staggered conformation for 2,2′-3,2′-[1,5-$C_2B_3H_4$]$_2$-1,5-$C_2B_3H_3$. Each closed circle represents CH and each open circle BH or B.

Table III. Vibrational Spectra of 2,2′-[1,5-$C_2B_3H_4$]$_2$

IR[a]	Raman[a]	IR	Raman
	549 w		1127 s
	571 w		1130 sh
	575 sh	1199 mb	
	651 vwb	1208 wb	
	786 sh	1284 wb	1284 w
	788 w		1290 sh
798 sh			1350 w
805 w			1352 sh
810 sh	810 w		1374 w
	812 sh	2520 vvw	
	840 wb	2560 vvw	
857 mb			2604 sh
907 sh		2614 sh	2614 sh
910 m			2616 mP
912 sh			2618 sh
	972 w	2620 vs	
	975 sh		2623 sh
1083 sh		2632 sh	
1100 sh		2660 sh	
1106 vs			3149 sh
	1104 s		3151 mP
1110 sh		3158 vvwb	3158 sh
1118 sh	1116 vs		

[a] Frequencies in cm^{-1}; w = weak, m = medium, s = strong, v = very, sh = shoulder, b = broad, P = polarized.

Although the NMR data defines the primary structures of $C_4B_6H_8$ and $C_6B_9H_{11}$ as the dimer and trimer of $C_2B_3H_5$, it does not define the relative orientation of the cages with respect to each other. Assuming that there is no free rotation around the exopolyhedral BB bond (justified a posteriori), the two limiting structures of the dimer are shown in Figure 1. The "staggered" conformation has D_{2d} symmetry while the "eclipsed" has D_{2h} symmetry. Intermediate conformations would have D_2 symmetry. Similarly, a number of conformations are possible for the trimer, one of which is shown in Figure 2.

In an attempt to distinguish between the possible conformations of the dimer the IR and Raman spectra were recorded and are presented in Table III. Assuming that the dimer has either the D_{2d} or D_{2h} structure, simultaneous Raman and infrared activity is permitted for the B_2 and E vibrations of the D_{2d} structure, whereas for the D_{2h} structure coincidences between Raman lines and infrared bands can only be accidental (the rule of mutual exclusion).[35] A cursory examination

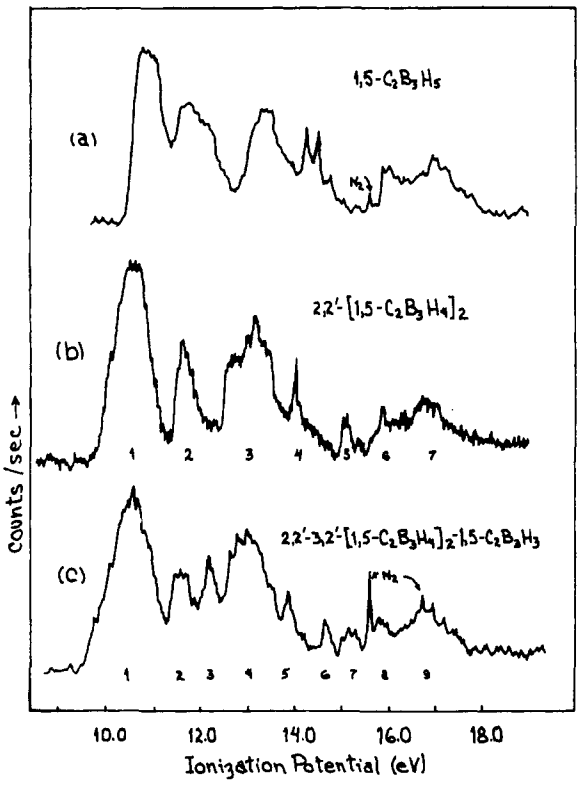

Figure 3. The He(I) photoelectron spectra of (a) 1,5-$C_2B_3H_5$, (b) 2,2'-[1,5-$C_2B_3H_4$]$_2$, and (c) 2,2'-3,2'-[1,5-$C_2B_3H_4$]$_2$-1,5-$C_2B_3H_3$.

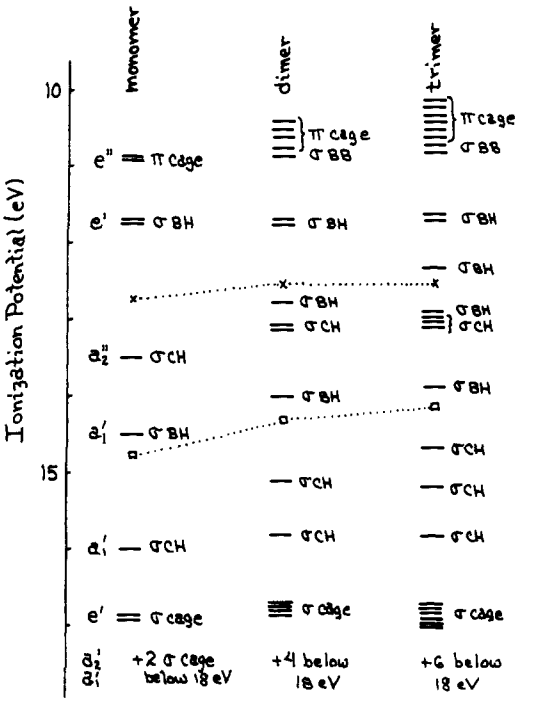

Figure 4. A correlation diagram relating the photoelectron spectra of the dimer and trimer to that of the monomer (1,5-$C_2B_3H_5$). The x refers to the center of gravity of the exo (BH) ionizations while the □ refers to that of the exo (CH) ionizations.

of Table III shows a number of coincidences of bands in the Raman and infrared spectra. This suggests that the molecule does not possess a center of inversion; i.e., the structure is D_{2d}.

This conclusion is supported by a closer examination of the CH stretching region. For reference 1,5-$C_2B_3H_5$ exhibits two CH stretches: 3158 cm^{-1} in the Raman assigned to A_1' and 3165 cm^{-1} in the IR assigned to A_2''.[36] For both dimer structures we expect four CH stretches. For the D_{2d} dimer they have the symmetries A_1, B_2, and E all of which are Raman active, the B_2 and E being IR active and the A_1 polarized in the Raman. For the D_{2h} dimer the vibrations will be A_g, B_{3g}, B_{1u}, and B_{2u} with the first two being Raman active and the last two IR active. Again the symmetric A_g vibration will be polarized in the Raman. Comparison of parallel and perpendicular polarization data on the peak centered at 3151 cm^{-1} shows the presence of three absorptions one of which is polarized. The fact that three bands are observed and that there is a coincidence between one of these and the very weak band in the IR implies that the molecular symmetry is D_{2d} rather than D_{2h}. The examination of the BH stretching region also revealed one polarized band, but the presence of isotopic bands (20% ^{10}B) did not permit a similar analysis. Because of the possibility of accidental degeneracies or a breakdown of selection rules, the IR–Raman comparison cannot be taken as definitive structural evidence, but it certainly suggests the D_{2d} configuration for the dimer and, consequently, implies a fairly large barrier of rotation around the exopolyhedral boron–boron bond as well as a significant interaction between the cages joined by this bond.

Photoelectron Spectra. The photoelectron spectra of 1,5-$C_2B_3H_5$, 2,2'-[1,5-$C_2B_3H_4$]$_2$, and 2,2'-3,2'-[1,5-$C_2B_3H_4$]$_2$-1,5-$C_2B_3H_4$ are presented in Figure 3 and the numerical data for the last two molecules are gathered in Tables IV and V.

The empirical interpretation of the spectra for the dimer and trimer are based on an analysis of 1,5-$C_2B_3H_5$. This molecule has been discussed previously[31] and a line representation of the observed ionization potentials and assignments is given at the left of Figure 4. This assignment is considered established (see Experimental Section).

For the dimer we expect 12 endo orbitals (4π and 8σ) and 9 exo orbitals (4 BH σ, 4 CH σ, and 1 BB σ).[37] Independently of whether the interaction between the individual cages is large or small, we expect the various classes of orbitals, with the exception of the new exo BB orbital, to have approximately the same centers of gravity in terms of energy as in the monomer; i.e., the dimer orbital structure is built up from the orbitals associated from two monomer fragments. This, along with the relative band areas, leads directly to the empirical assignments given in Table IV and Figure 4 except that the location of the exo (BB) orbital is not defined. In terms of band areas it may lie either in band 1 or 3.

This basic assignment of the spectrum is supported by comparison with the calculated MNDO eigenvalues and predominant atomic character given in Table IV for the D_{2d} structure. None of the MOs is "pure" in character; however, with the exception of the exo (CH) orbital discussed in the Experimental Section, the agreement between experimental and theoretical assignments is good provided that the BB ionization is placed in band 1. For the D_{2d} calculation the center of gravity of the predominantly BH MOs is 14.05 eV while that for the CH MOs is 15.28 eV. The experimental numbers are 12.6 and 14.3 eV. Corresponding numbers for 1,5-$C_2B_3H_5$ are 13.92 (BH)/15.22 (CH) calculated and 12.7 (BH)/14.7 (CH) experimental.[31] The calculated distribution of eigenvalues for the dimer with D_{2h} symmetry is qualitatively similar in terms of MO character. However, the eigenvalues derived from the uppermost e MOs of D_{2d} symmetry split significantly into four nondegenerate MOs in D_{2h} and this will be important to the discussion below.

The natures of the first two bands in the observed photoelectron spectrum have structural implications concerning the relative orientation of the monomer units across the exo BB bond. The width of band I in the dimer (0.85 eV fwhm) is not much larger than that of band 1 in the monomer (0.75 eV

Table IV. Ionization Potentials, Band Areas, and Assignments for 2,2′-[1,5-$C_2B_3H_4$]$_2$

band[a]	IP[b] eV	A/E[c] (rel)	IP per band, band character (empirical)	MNDO $-\epsilon_i$, eV	MNDO symmetry D_{2d}	MNDO character[d]
1	10.4 sh	1.0	4 endo π	11.33	e	endo π
	10.7		1 exo BB	11.53	a_2	endo π
				11.53	b_1	endo π
				11.79	a_1	exo BB
2	11.7	0.4	2 exo BH	12.70	e	exo BH with some CH
3	12.6 sh	1.1	1 exo BH	14.14	b_2	exo BH and some BB*
	13.1		2 exo CH			
				13.12	e	exo CH with BH
4	14.0	0.2	1 exo BH	16.66	a_1	exo BH
5	15.1		1 exo CH	17.41	b_2	exo CH
6	15.8		1 exo CH	17.47	a_1	exo CH
7	16.7		4 endo σ	18.25	b_2	endo B_{2s}[e]
				19.77	e	endo B_{2s}[e]
				21.61	a_1	endo B_{2s}[e]
	>19		4 endo σ	27.76	e	endo C_{2s}[e]
				40.30	b_2	endo C_{2s},B_{2s}[e]
				40.56	a_1	endo C_{2s},B_{2s}[e]

[a] See Figure 3 for numbering. [b] Energies refer to band centers. Shoulders on bands are indicated by sh following the energy. [c] Relative area divided by electron energy. [d] Determined from largest orbital coefficients. [e] These orbitals contain sufficient H1s character to make this designation arbitrary.

Table V. Ionization Potentials, Band Areas, and Assignments for 2,2′,3,2′-[1,5-$C_2B_3H_4$]$_2$-1,5-$C_2B_3H_3$

band[a]	IP,[b] eV	A/E[c] (rel)	IP per band, band character (empirical)	$-\epsilon_i$, eV, MNDO staggered-staggered
1	9.9 sh	1.0	6 endo π	11.16
	10.2 sh		2 exo BB	11.25
	10.6			11.29
	10.8 sh			11.44
				11.52
				11.52
				11.87
				12.30
2	11.7	0.3	2 exo BH	12.54
				12.94
3	12.2	0.3	1 exo BH	13.74
4	13.0	0.8	3 exo CH	12.97
			1 exo BH	12.97
				13.17
				14.71
5	13.9	0.1	1 exo BH	16.72
6	14.7		1 exo CH	17.36
7	15.2		1 exo CH	17.44
8	15.8		1 exo CH	17.48
9	16.8		6 endo σ	17.82-21.91
	>19		6 endo σ	27.75-40.60

[a] See Figure 3 for numbering. [b] Energies refer to band centers. [c] Relative area divided by electron energy.

fwhm). As in both cases the bands result from the endo π framework ionizations, there must be little perturbation of the endo π orbitals of one monomer unit by the endo π orbitals on the other. As portrayed in the sketches of Figure 5, each noninteracting monomer unit has two endo π framework orbitals (the degenerate e″ pair in the monomer). If the dimer structure were D_{2h} (or D_2), then a π-type interaction between filled orbitals (a) on each monomer unit is possible. The other component on each monomer will remain nonbonding as it has a node at the position of attachment. As indicated at the right of Figure 5, this will lead to a splitting, ΔE, between the bonding and antibonding orbitals formed from the interacting monomer orbitals.[38] But, as pointed out above, no significant splitting is observed. Therefore, either ΔE is small or the

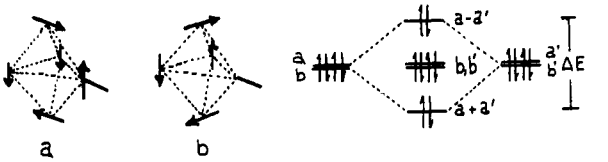

Figure 5. The e″ endo π surface orbitals and the filled orbital π–π interaction expected in the D_{2h} conformation.

structure of the dimer is D_{2d}. We have demonstrated in past work[19,20] that the interaction between filled endo π framework orbitals and exopolyhedral substituents containing filled π-type orbitals is not small and, assuming a similar interaction constant in this case, we would predict that for the D_{2h} structure ΔE should be about 1–2 eV. Therefore, we suggest that as no interaction is observed it is symmetry forbidden; i.e., the structure is D_{2d}. This interpretation is supported by the MNDO calculations, which yield widths of the eigenvalue distributions corresponding to band 1 of 0.0 eV in the monomer, 0.46 eV in the D_{2d} dimer (Table IV), and 1.4 eV in the D_{2h} dimer. The latter value results from the splitting of the HOMO e eigenvalue in D_{2d} symmetry into b_{1u} and b_{3g} in D_{2h} symmetry, with calculated eigenvalues of −10.70 and −12.11 eV, respectively.

The second band that is structurally important is band 2 in the dimer. For both limiting structures, D_{2d} and D_{2h}, four exo BH orbitals are expected. In the case of the D_{2d} structure they will have the symmetries a_1, b_2, and e as schematically indicated in Figure 6. In going to the D_{2h} structure the degenerate e pair splits into orbitals of b_{3u} and b_{1g} symmetry as also indicated in Figure 6. Band 2 contains two exo BH ionizations and it is quite sharp. Therefore, either the b_{3u} and b_{1g} orbitals are accidentally degenerate or the band corresponds to the ionization of the e orbitals of the D_{2d} structure. The former is not impossible, but the MNDO calculations show that the degenerate e MO at −12.70 eV is split into b_{1g} and b_{3u} exo BH orbitals in the D_{2h} structure at −12.27 and −12.97 eV, respectively. A splitting of this magnitude (0.7 eV) would be observable. Again the D_{2d} structure is suggested.

The empirical assignment of the trimer was carried out similarly to that of the dimer. The results are presented in Figure 4 as well as in Table V.[39] Also given in Table V are the MNDO results for the trimer in the staggered-staggered C_{2v}

Table VI. Calculated Molecule and Bond Properties for 2,2′-[1,5-$C_2B_3H_4$]$_2$

twist angle, deg	$\Delta H_f°$, kcal/mol	d(BB), Å	HOMO, eV	bond order: HOMO x–x	bond order: HOMO z–z	bond order: total x–x	bond order: total z–z
0 (D_{2h})	53.26	1.626	−10.70	0.000	−0.236	0.106	0.138
10	53.03	1.625	−10.71	0.001	−0.231	0.110	0.140
20	52.34	1.620	−10.74	0.004	−0.218	0.118	0.146
30	51.30	1.614	−10.78	0.007	−0.198	0.132	0.154
40	50.03	1.606	−10.84	0.010	−0.171	0.148	0.165
50	48.69	1.600	−10.92	0.011	−0.140	0.164	0.176
60	47.42	1.591	−11.01	0.010	−0.106	0.179	0.185
70	46.39	1.585	−11.11	0.007	−0.072	0.190	0.193
80	45.71	1.582	−11.22	0.001	−0.038	0.198	0.199
90 (D_{2d})	45.47	1.581	−11.33	−0.012	−0.012	0.200	0.200

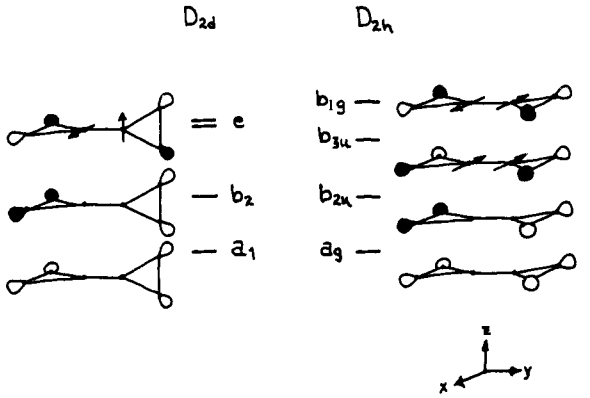

Figure 6. A representation of the exo (BH) orbitals of the dimer in D_{2d} and D_{2h} conformations.

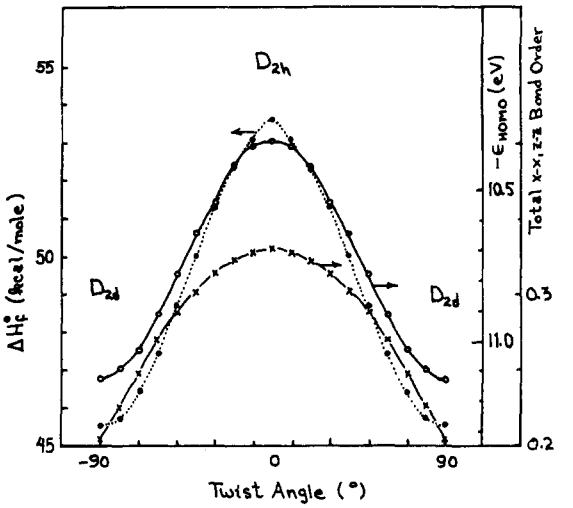

Figure 7. A plot of the heat of formation (●), HOMO energy (x), and total x–x and z–z bond order (○) as a function of twist angle.

(Figure 2) conformation. Comparison of the calculated eigenvalues and the photoelectron spectrum is not as straightforward as for the monomer and dimer because of the large number of MOs and the increased extent of mixing of AO components into each MO. A rough assignment of orbital character yields calculated centers of gravity of 14.13 (BH)/15.23 (CH) in agreement with the experimental values of 12.5 (BH)/14.1 (CH).

The calculations show that the first six orbitals are to be associated with the endo π surface orbitals of the three cages. Thus, the fact that the width of band 1 (1.05 eV fwhm) is not much larger than that of the dimer and monomer can again be taken as evidence of little perturbation of the filled endo π surface orbitals on the three monomer units. The same argument, presented above for the dimer, leads to the suggestion that the staggered-staggered conformation in Figure 2 is adopted by the trimer. This conclusion is supported by the MNDO calculations (Table V) in that the net spreads of the eight orbitals assigned to band 1 are 1.14 eV in the staggered-staggered conformation, 1.43 eV for the staggered-eclipsed conformation, and 1.72 eV for the eclipsed-eclipsed conformation.

Intercage Interaction. As the exopolyhedral B–B bond is ostensibly a single bond, the preference of the coupled cage systems for a staggered arrangement implies the existence of a force acting between the cages. Besides corroborating the assignment of the photoelectron spectra and supporting the structural interpretation of these spectra, quantum-chemical calculations allow the origin of this intercage interaction to be explored.

The MNDO technique is useful as it allows a number of structurally relevant properties to be calculated. The properties pertinent to this discussion are tabulated in Table VI for the dimer as a function of twist angle around the exopolyhedral B–B bond as the conformation is changed from D_{2h} to D_{2d}. As shown in Figure 7, the D_{2h} conformation constitutes a maximum in energy as a function of angle. At the same time the exo B–B length is a maximum in the D_{2h} conformation. The qualitative result as well as the magnitude of the energy change agrees very well with the structural conclusion based on spectroscopy. Variation in orbital and bond properties, also contained in Table VI, allows the factors that determine the preferred structure to be explored.

First we focus attention on the HOMO and its variation as a function of twist angle. The simple filled orbital model presented in Figure 5 and discussed in conjunction with the photoelectron spectrum suggests that the HOMO for the D_{2h} conformation consists in the antibonding combination of an endo π surface orbital from each cage. As the dimer is twisted to yield the D_{2d} conformation both the filled orbital interaction and the HOMO energy will decrease. The MNDO results (Table VI) do indeed show that the HOMO stabilizes as a function of twist angle. In fact the angular dependence of the heat of formation, the B–B bond length, the HOMO energy, and the z–z bond order term of the HOMO have the same qualitative variation with twist angle. Of even more interest is that the sums of the orbital energies for the lowest 20 of the 21 occupied MOs are −379.33 eV for D_{2h} and −379.28 eV for D_{2d} symmetry. Thus, in the sense of a Walsh diagram, the energy of the HOMO correctly reflects the energy of the molecule as a function of geometry.

It is possible that the strong filled orbital interaction predicted for the D_{2h} geometry and verified in the MNDO calculations is actually responsible for the barrier of Figure 7. This is investigated by examining all the bond order terms. Summing up all the σ B–B bond order terms we obtain 1.86 for D_{2h} and 1.87 for D_{2d} showing that, as expected, the σ interactions are not responsible for the barrier. On the other hand, the *total* x–x and z–z[40] bond-order terms (Table VI)

Table VII. Calculated Molecule and Bond Properties for 2,2'-3,2'-[1,5-$C_2B_3H_4$]$_2$-1,5-$C_2B_3H_3$

structure	$\Delta H_f°$, kcal/mol	d(B-B), Å	HOMO, eV	BB bond order z-z term[a]
eclipsed-eclipsed	79.71	1.626	−10.55	0.138
C_{2v}				0.138
eclipsed-staggered	71.98	1.581	−10.70	0.138
C_s		1.627		0.200
staggered-staggered	64.33	1.582	−11.16	0.199
C_{2v}				0.199
(Figure 2)				

[a] z is perpendicular to the plane formed by the three boron atoms of the central cage.

increase with twist angle, and when we examine the dependence of this quantity on twist angle (Figure 7) it is found to be quite similar to that observed for the heat of formation. Thus, it is clear that the origin of the preference for the D_{2d} geometry lies in π-π interactions between the two cages, but is not restricted to the HOMO behavior.[41]

By examining individual terms in the bond-order sums, we find that the major changes in x-x and z-z bond orders between D_{2d} and D_{2h} geometries lie in the orbital pairs that have e symmetry in the D_{2d} structure. One such pair contains the HOMO discussed above. But in fact this particular pair does not appear crucial in the total. In D_{2h} geometry the corresponding bonding combination (see Figure 5) has a bond-order term that practically cancels that of the antibonding combination (−0.236 vs. 0.214) while in D_{2d} geometry these orbitals are nearly nonbonding. Instead, the key to geometrical control lies in the next two pairs, e(BH) and e(CH) in D_{2d} symmetry (Table IV). The former pair is represented in Figure 6, from which it is evident that each member contains a B $2p_x$ contribution (e(CH) will contain B $2p_z$). In D_{2h} symmetry the b_{3u} component will be x-x bonding across the B-B bond while the b_{1g} will be antibonding. Taking independent axes in each cage for the moment, the 90° twist to produce D_{2d} symmetry will uncouple the x-x components; however, they *will couple* to the totally analogous z components of e(CH). In D_{2h} the sum of the four π bond order terms is 0.204 while for D_{2d} it is 0.352, showing that the four cross terms in D_{2d} outweigh the two bonding minus the two antibonding terms in D_{2h}.

This "answer" to the question of geometrical preference is also physically reasonable. The monomer unit, 1,5-$C_2B_3H_5$, has a long boron-boron distance in the cage (1.853 Å)[42] and a theoretical study shows that the classical structure below, in

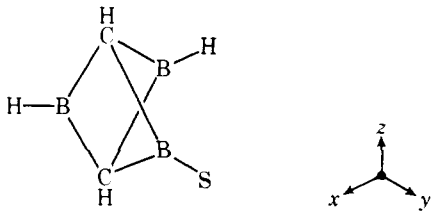

which each boron is three coordinate, is a good representation of the bonding.[30] Clearly, the monomer unit does not fully utilize the B $2p_x$ orbitals in bonding and, thus, the D_{2d} geometry of the dimer permits an interaction between the underutilized B $2p_x$ orbitals and the highly utilized B $2p_z$ orbitals of each cage. In a real sense then the D_{2d} geometry maximizes two π-π filled-unfilled interactions for each π-π bonding and antibonding interaction maximized in the D_{2d} geometry. This interpretation is summarized in Figure 8b.

To further explore the geometry as a function of electronic structure, calculations were carried out on the 2+ and 2− ions. In each case the D_{2h} conformer is predicted to be more stable. The prediction of D_{2h} geometry for the doubly charged ions

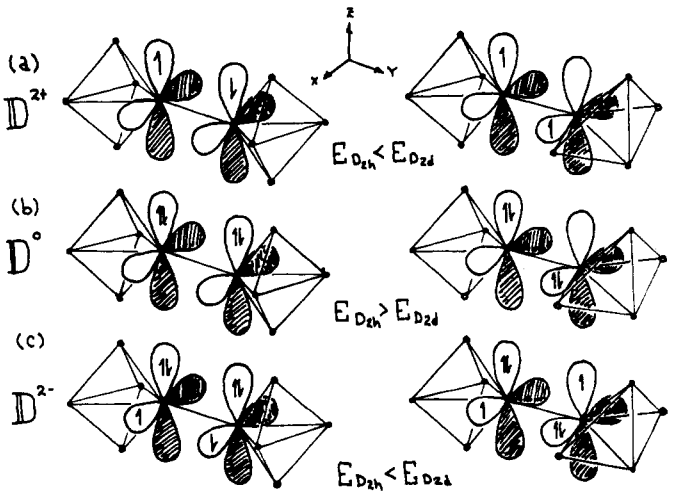

Figure 8. A representation of the major π interactions between two coupled 1,5-$C_2B_3H_5$ cages.

is entirely expected if π-π interactions across the exopolyhedral B-B bond are the controlling factor. Figure 8 presents a schematic, highly simplified explanation in terms of the $2p_x$ and $2p_z$ orbitals of the boron atoms linking the two cages. In forming the 2+ ion, the antibonding orbital in Figure 5 is emptied so that a net π z-z bonding interaction is gained in D_{2h} over D_{2d} (a). In the 2− ion the additional electrons populate the B $2p_x$ orbitals, thereby introducing a π x-x bonding interaction in D_{2h} but not in D_{2d} geometry.

The results of the MNDO calculation on the trimer in three conformations are given in Table VII. Based upon the knowledge gleaned from the dimer, the results for the trimer are understandable. Each succeeding twist of a cage saves the molecule about 8 kcal/mol of energy as found for the dimer. The B-B bond lengths, HOMO energy, and B-B bond order terms also closely parallel the values found in the calculations on the dimer. Thus, the calculations support the structure given in Figure 2 as the proposed structure for the trimer.

Conclusions

It is demonstrated that coupled 1,5-$C_2B_3H_5$ cages display a type of fixed geometry with respect to the exopolyhedral B-B bond that is unanticipated on the basis of simple σ bonding considerations. The geometries adopted by the dimer and trimer result from a π-type interaction of the orbitals associated with each individual cage. Basically, the substantial barrier to rotation around the B-B bond can be traced to an underutilization of the B $2p_x$ orbitals compared to the B $2p_z$ orbitals in the individual monomer cages. The work shows that not only are π-type surface orbitals important in terms of understanding intracage bonding and cage substituent effects, but they are also important in terms of intercage geometry. As no boron cage fully utilizes its 2p orbitals, it will be of interest to see whether similar intercage geometrical effects carry over to other coupled cage systems.

Acknowledgments. We thank the National Science Foundation (Grant CHE78-11600) for the support of this work and the University of Notre Dame Computer Center for providing computing time.

References and Notes

(1) Department of Chemistry, Calvin College, Grand Rapids, Mich. 49506.
(2) Grimes, R. N.; Wand, F. E.; Lewin, R.; Lipscomb, W. N. *Proc. Natl. Acad. Sci. USA.* **1961**, *47*, 996.
(3) Dobson, J.; Gaines, D. F.; Schaeffer, R. *J. Am. Chem. Soc.* **1965**, *87*, 4072.
(4) Steck, J.; Pressley, G. A., Jr.; Stafford, R. E.; Dobson, J.; Schaeffer, R. *Inorg. Chem.* **1969**, *8*, 830.
(5) Gaines, D. F.; Iorns, T. V.; Clevenger, E. N. *Inorg. Chem.* **1971**, *10*,

1096.
(6) Maruca, R.; Schaeffer, R. *Inorg. Chem.* **1970**, *9*, 2161.
(7) Hall, L. H.; Koski, W. S. *J. Am. Chem. Soc.* **1962**, *84*, 4205.
(8) Boocock, S. K.; Greenwood, N. N.; Kennedy, J. P.; Taylorson, D. *J. Chem. Soc., Chem. Commun.* **1979**, 16. Greenwood, N. N.; Kennedy, J. D.; McDonald, W. S.; Staves, J.; Taylorson, D. *Ibid.* **1979**, 17.
(9) Greenwood, N. N.; Kennedy, J. D.; Spalding, T. R.; Taylorson, D. *J. Chem. Soc., Dalton Trans.* **1979**, 840.
(10) Brown, G. M.; Pinson, J. W.; Ingram Jr., L. L. *Inorg. Chem.* **1979**, *18*, 1951.
(11) DuPont, J. A.; Hawthorne, M. F. *J. Am. Chem. Soc.* **1964**, *86*, 1643.
(12) Hawthorne, M. F.; Owen, D. A. *J. Am. Chem. Soc.* **1968**, *90*, 5912.
(13) Burg, A. B.; Reilly, T. J. *Inorg. Chem.* **1972**, *11*, 1962.
(14) Plotkin, J. S.; Sneddon, L. G. *J. Chem. Soc., Chem. Commun.* **1976**, 95.
(15) Pretzer, W. R.; Rudolph, R. W. *Inorg. Chem.* **1976**, *15*, 1779.
(16) Dobble, R. C.; Distefano, E. W.; Black, M.; Leach, J. B.; Onak, T. *J. Organomet. Chem.* **1976**, *114*, 233.
(17) Plotkin, J. S.; Astheimer, R. J.; Sneddon, L. G. *J. Am. Chem. Soc.* **1979**, *101*, 4155.
(18) Hosmane, N. S.; Grimes, R. N. *Inorg. Chem.* **1979**, *18*, 2886.
(19) Ulman, J. A.; Fehlner, T. P. *J. Am. Chem. Soc.* **1976**, *98*, 1119.
(20) Beltram, G. A.; Fehlner, T. P. *J. Am. Chem. Soc.* **1979**, *101*, 6237.
(21) Fehlner, T. P. *Inorg. Chem.* **1975**, *14*, 934.
(22) Shriver, D. F. "The Manipulation of Air-Sensitive Compounds"; McGraw-Hill: New York, 1969.
(23) Klein, M. J.; Harrison, B. C.; Solomon, I. J. *J. Am. Chem. Soc.* **1958**, *80*, 4149.
(24) First reported by Burg and Reilly, ref 13.
(25) An uncharacterized white solid was also observed by Burg and Reilly, ref 13.
(26) The reaction of 1,5-$C_2B_3H_5$ with $Fe(CO)_5$ yields $C_2B_3H_5Fe(CO)_3$ among other products: Miller, V. R.; Sneddon, L. G.; Beer, D. C.; Grimes, R. N. *J. Am. Chem. Soc.* **1974**, *96*, 3090.
(27) Dewar, J. S.; Thiel, W. *J. Am. Chem. Soc.* **1977**, *99*, 4899. Thiel, W. *QCPE* **1978**, *11*, 353.
(28) Dewar, M. J. S.; McKee, M. L. *J. Am. Chem. Soc.* **1977**, *99*, 5231.
(29) Guest, M. F.; Hillier, I. H. *Mol. Phys.* **1973**, *26*, 435.
(30) Dixon, D. A.; Kleier, D. A.; Halgren, T. A.; Hall, J. H.; Lipscomb, W. N. *J. Am. Chem. Soc.* **1977**, *99*, 6226.
(31) Ulman, J. A.; Fehlner, T. P. *J. Am. Chem. Soc.* **1978**, *100*, 449.
(32) Rabalais, J. W. "Principles of Ultraviolet Photoelectron Spectroscopy"; Wiley-Interscience: New York, 1977.
(33) Dewar, M. J. S.; McKee, M. L. *Inorg. Chem.* **1978**, *17*, 1569.
(34) Onak, T.; Wan, E. *J. Chem. Soc., Dalton Trans.* **1974**, 665.
(35) Wilson, E. B., Jr.; Decius, J. C.; Cross, P. C. "Molecular Vibrations"; McGraw-Hill: New York, 1955.
(36) Jotham, R. W.; Reynolds, D. J. *J. Chem. Soc. A* **1971**, 3181.
(37) σ and π refer to the symmetry of the orbital with respect to the radial direction of an exopolyhedral bond. This designation can be ambiguous. For example, in $B_6H_6^{2-}$, the t_{2g} orbitals interact with exopolyhedral ligands in a π fashion only while the t_{1u} orbitals can interact in both σ and π fashions. It is found in terms of PES (ref 20) that the t_{1u} π interaction is relatively small; hence only the t_{2g} orbitals were considered as π orbitals. As the latter are constructed mainly of p functions that are tangential to the surface of the sphere that holds the cage atoms, we also refer to these orbitals as surface orbitals.
(38) Note that, as one-half of the D_{2h} dimer is twisted, the bonding and antibonding components will become degenerate.
(39) As the symmetry becomes lower this type of assignment becomes more arbitrary and less meaningful, especially in terms of the exo σ and endo σ designations.
(40) See Figure 6 for the axes used.
(41) The HOMO shows little variation in the x–x bond order, but the totals in Table VI show this interaction to be important.
(42) McNeill, E. A.; Gallaher, K. L.; Scholer, F. R.; Bauer, S. H. *Inorg. Chem.* **1973**, *12*, 2108.

Electron Spin–Echo Studies of Radical Interaction and Orientation on Catalytic Surfaces. CH_2OH Radicals in A-, Y-, and X-Type Zeolites

Tsuneki Ichikawa and Larry Kevan*

Contribution from the Department of Chemistry, Wayne State University, Detroit, Michigan 48202. *Received October 10, 1979*

Abstract: CH_2OH radicals have been generated by γ-radiolysis at 77 K from methanol adsorbed on Na-A, Na-Y, Na-X, and K-X type zeolites. The electron spin resonance spectra of the radicals on the different zeolites are similar. However, electron spin-echo modulation patterns associated with aluminum nuclei in the zeolites are observed at 4 K and show differences between the different zeolites. These spin-echo results have been simulated in order to obtain structural information about the adsorbed radical site. Each radical interacts with one Si or Al nucleus at 3.4 Å in Na^+-containing zeolites and at 3.6 Å in K^+-containing zeolites. From these data and from structural data on the zeolites the CH_2OH radical is suggested to be located in an α cage with its molecular dipole oriented toward a cation in the center of the square (X and Y zeolite) or hexagonal (A zeolite) faces of the α cage. The COH plane is aligned along a diagonal of the square face so that the radical site is oriented toward one Al or Si nucleus. The utility of electron spin-echo modulation analysis to probe the orientation of adsorbed species relative to the surface is emphasized.

Introduction

The characterization of the structure of reactive intermediates adsorbed on surfaces is of major importance for elucidation of the chemical pathways in heterogeneous catalysis. For paramagnetic intermediates electron spin resonance (ESR) is a primary method of characterization. Extensive work has been carried out in this area,[1] the general focus of which has been to measure deviations of radical hyperfine parameters for radicals adsorbed on surfaces compared to radicals trapped in bulk solids. These changes in hyperfine parameters have typically been interpreted in terms of a change in the radical structure itself or in its electron distribution due to strong surface electric fields. Although interesting and significant, such studies have not generally led to information about the orientation and interaction distances of the radicals *relative to the surface atoms*. Such information is potentially contained in hyperfine interactions which are usually too weak to be seen in normal ESR experiments.

In the last several years we have shown that the weak hyperfine interactions characterizing the average surroundings of a trapped radical in a *disordered matrix* can often be quantitatively analyzed from electron spin-echo modulation patterns.[2-4] In particular, the *detailed* solvation geometry of solvated electrons[2,3,5-8] and of selected anions,[9] atoms,[10-12] and cations[13] in frozen solutions has been elucidated for the first time. In general, one can identify the type, number, distance, and isotropic hyperfine coupling of magnetic nuclei within about 2–6 Å from the unpaired electron on a radical.[14]

Here, we show how electron spin-echo modulation analysis can be applied to study the local environment of radicals ad-

0002-7863/80/1502-2650$01.00/0